Geopersia ***9*** *(2), 2019, PP. 395-410* *DOI: 10.22059/GEOPE.2019.269872.648430*

Pore throat size characterization of carbonate reservoirs by integrating core data, well logs and seismic attributes

Sirous Hosseinzadeh[1], Ali Kadkhodaie[2], Hossein Mossadegh[3]*, Rahim Kadkhodaie Ilkhchi[2]
[1] *Oil and Energy Petropars Company, Tehran, Iran*
[2] *Earth Science Department, Faculty of Natural Science, University of Tabriz, Tabriz, Iran*
[3] *Department of Geology, Kharazmi University, Tehran, Iran*
**Corresponding author, e–mail: kadkhdaie_ali@tabrizu.ac.ir*
(*received: 19/11/2018 ; accepted: 24/04/2019*)

Abstract
The current study proposes a three-step approach for pore throat size characterization of these reservoirs, by integrating core data, well logs and 3D seismic volume. In this respect, first the pore throats size was calculated using Pittman and Winland models based on routine core analysis data and calibration the results with the laboratory-derived capillary pressure curves. In the second step, the pore throat size as a continuous log was calculated using petrophysical data for each studied well. Finally, the calculated pore throat size log was tied to 3D seismic data at well locations. The results show that seismic attributes including acoustic impedance, amplitude envelope, filter 15/20-25/30 and derivative instantaneous amplitude are the best predictor set for converting the 3D seismic volume into a pore size cube by a probabilistic neural network mode. The methodology illustrated in this study, was employed on Ilam carbonate reservoir in one of the southwestern oilfields of Iran. The findings demonstrate that seismic data in combination with core and well log data could be considered as an effective tool for spatial modeling and characterization of pore throat size in carbonate reservoirs.

Keywords: *Pore Throat Size, Artificial Neural Network, Seismic Attributes, Seismic Inversion, Carbonate Reservoirs.*

Introduction

Estimation of production performance in a heterogeneous reservoir is not possible without an accurate calculation of physical properties of reservoir rocks. Permeability that is a measure of the rock capability for transmission of fluids (Tiab & Donaldson, 2015) has an important effect on reservoir performance. In addition, textural characteristics of reservoir rocks such as grain size and sorting have significant control on permeability, porosity, enhancement oil recovery and capability of maintaining the hydrocarbon column by cap rock (Rezaee *et al*., 2006; Buryakovsky *et al*., 2012; Tiab & Donaldson, 2015). In the process of water replacement by oil in a water-wet system, first the displacement process occurs in a small segment that reduces the oil continuity, and leaves bobbles of residual oil in pore throat size; so, residual oil volume depends on pore and pore throat size (Wardlaw *et al*., 1987; Scott & Barker, 2003; Nelson, 2009; Rezaee *et al*., 2006). Therefore, study of physical properties of reservoir rocks through analysis of core data and petrophysical well logs is essential to reach a comprehensive understanding of reservoir production behavior in the field. Also, seismic data are being successfully applied to predict the reservoir rock properties (Russel, 2004; Shahraeeni *et al*., 2012; Yarmohammadi *et al*., 2014; Grana & Rossa, 2010; Bosch *et al*., 2010; Bornard *et al*., 2005; Dai *et al*., 2004; Dorrington & Link, 2004; Dolberg *et al*., 2000).This study with focus on a carbonate reservoir from one of the fields of southwestern Iran pursues the following targets.

a) Investigation the pore throat size of the reservoir using core analysis data,
b) Determination of the optimized pore throat size relationship through analysis of Washburn, Pittman and Winland equations,
c) Prediction of permeability through analysis of petrophysical data, and generating R35 as a continuous log in the studied wells, and
d) Extraction a cube of pore throat size (PTS) from 3D seismic data.

Geological setting

The studied field is located in the northern part of the Abadan Plain, 15-30 meters above sea level, in southwest of Khuzestan province, and about 50 km west of Ahvaz industrial city, southwestern Iran (Figure 1**Error! Reference source not found.**). The hydrocarbon type in the field is heavy oil (23 API). The field has an anticlinal structure with NW-SW azimuthal trend. The structure has a very low angle flank, with an area of approximately 65Km^2 and small closure of about 75m on the Sarvak horizon.

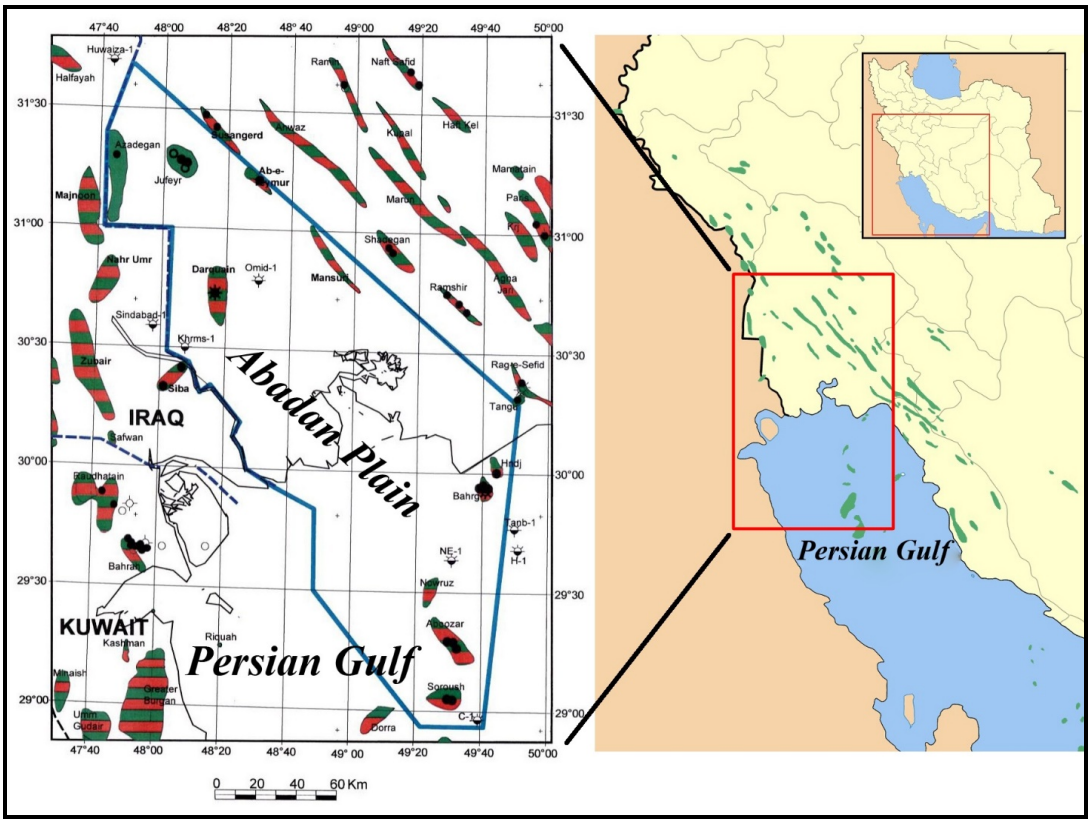

Figure 1. Location map of the studied field in SW of Iran (National Iranian Oil Company Report, 2009).

3D seismic data of the study area were acquired by Oil Exploration Operations Company (OEOC) in 2004. The main task of the 3D seismic survey was to specify the structural features of the reservoirs. As with the other structures in the Abadan Plain, the studied structure consists of several Cretaceous reservoirs including Ilam, Sarvak, Gadvan and Fahliyan formations (Figure 2). The target reservoir, upper Cretaceous Ilam Formation, consists of dark to light gray clay, limestone and shale (Mehrabi *et al*., 2014). This formation in this area is divided into five major zones including Ilam Zone, Ilam Upper-a, Ilam Upper-b, Ilam Main, and Ilam Poor. Among them, Ilam Upper-a and Ilam Main are considered as main reservoir zones. But, the other zones do not have good reservoir quality.

Methodology

In this study, core analysis data (42 SCAL and 213 CCAL) and conventional well logs from 3 wells of the studied field as well as 3D seismic data were integrated and used for pore throat size evaluation by applying the intelligent systems. Core intervals for the studied wells include Well #2 (2912-3016m), Well #3 (2930-3119m) and Well #5 (2972-3158m). A set of pre-calculations, environmental corrections and depth matching were applied on raw well log data to make them ready for interpretation. First, pore throat size was calculated based on empirical equations, and the results were compared with core analysis data. Afterward, it was tried to estimate permeability and pore throat size from petrophysical data by considering core results as reference. Finally, formulations were made between seismic attributes and pore throat radius using intelligent models to generate a 3D cube of pore throat size over the studied carbonate reservoir.

Estimation and evaluation of pore throat size based on empirical equations

Washburn Equation (Washburn, 1921)

Capillary pressure curves are one of the main sources for calculation of pore and pore throat radius distribution. Washburn (1921) found the relationship between capillary pressure and pore throat size in the form of Eq. (1).

$$P_c = \frac{2\sigma cos\theta}{r} \quad \text{Eq. (1)}$$

Where r is pore throat size (micron), σ: interfacial

tension (dyne/cm), θ: wetting phase angle (degree), P_c: capillary pressure (psi).

Capillary pressure data that are obtained from mercury injection test, porous diaphragm, dynamic method and centrifuge test, are represented as a plot of P_c versus non-wetting phase saturation. These data are measured usually with non-wetting fluids in laboratory condition. Accordingly, it is necessary to convert them from laboratory to reservoir conditions (Eq. 2 to Eq. 4).

$$P_{c(res)} = \frac{2\sigma_{res}Cos\theta_{res}}{r} \quad \text{Eq. (2)}$$

$$P_{c(lab)} = \frac{2\sigma_{lab}Cos\theta_{lab}}{r} \quad \text{Eq. (3)}$$

Since r=r

$$P_{c(res)} = \frac{2\sigma_{res}Cos\theta_{res}}{2\sigma_{lab}Cos\theta_{lab}} . P_{c(lab)} \quad \text{Eq. (4)}$$

Where subscripts "*res*" and "*lab*" represent Washburn parameters (Eq. 1) in reservoir and laboratory conditions, respectively.

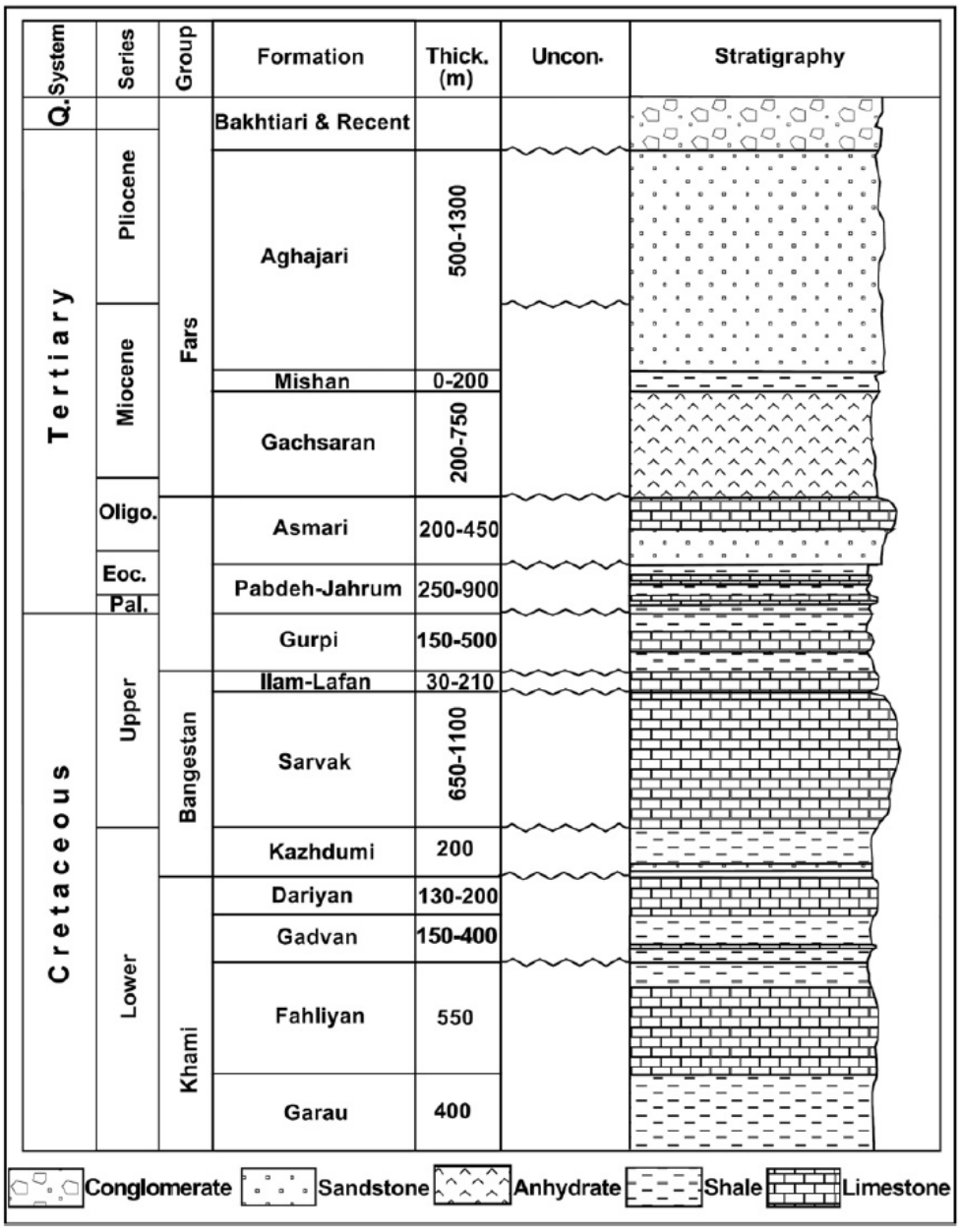

Figure 2. Cretaceous to Tertiary stratigraphy column of the study area (modified from Motiei 1993, Alavi 2004, and AbdollahieFard *et al.* 2006).

Winland Equation (Kolodzie, 1980):

Winland used the mercury capillary pressure curves for creating an empirical equation between porosity, permeability and pore throat size in reservoir rocks of the Spindale field. Winland equation uses capillary pressure data for real geometry of the pore throat size at 35% of non-wetting phase saturation (Eq. 5).

$$\text{Log R35} = 0.732 + 0.588*\log(K) - 0.864*\log(\varphi) \quad \text{Eq. (5)}$$

Where K is permeability (md), $\emptyset$ is porosity (%), and R35 is pore throat size (micron) at 35% of non-wetting phase saturation.

According to the cross plot of Figure 3, there is a high correlation coefficient (0.83) between Washburn and Winland pore throat size (R35) in the studied reservoir.

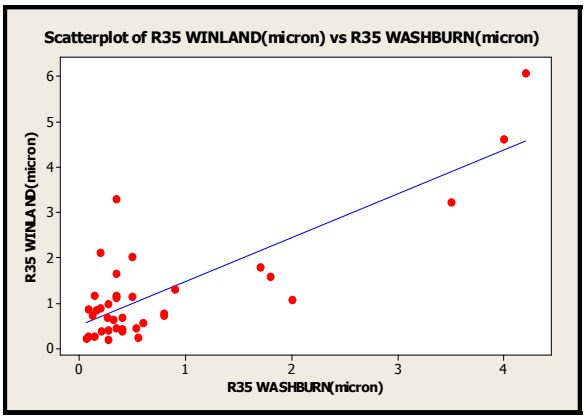

Figure 3. Correlation coefficient (R=0.83) between R35 from Washburn and Winland equations.

Pittman Equation (Pittman, 1992)

Winland equation in corrected samples for gas effect was tested by Pittman (1992) in the Ordovician clastic reservoirs. The studied sandstone samples were different in composition, texture and structure. Pittman equations for pore throat size determination based on different percentages of mercury saturation are listed in Eq. 6 to Eq. 19.

$$\text{Log (R10)} = 0.459 + 0.500*\log(K) - 0.385*\log(\varphi) \quad \text{Eq. (6)}$$

$$\text{Log (R15)} = 0.333 + 0.509*\log(K) - 0.344*\log(\varphi) \quad \text{Eq. (7)}$$

$$\text{Log (R20)} = 0.218 + 0.519*\log(K) - 0.303*\log(\varphi) \quad \text{Eq. (8)}$$

$$\text{Log (R25)} = 0.204 + 0.531*\log(K) - 0.350*\log(\varphi) \quad \text{Eq. (9)}$$

$$\text{Log (R30)} = 0.215 + 0.547*\log(K) - 0.420*\log(\varphi) \quad \text{Eq. (10)}$$

$$\text{Log (R35)} = 0.255 + 0.565*\log(K) - 0.523*\log(\varphi) \quad \text{Eq. (11)}$$

$$\text{Log (R40)} = 0.360 + 0.582*\log(K) - 0.680*\log(\varphi) \quad \text{Eq. (12)}$$

$$\text{Log (R45)} = 0.609 + 0.608*\log(K) - 0.974*\log(\varphi) \quad \text{Eq. (13)}$$

$$\text{Log (R50)} = 0.778 + 0.626*\log(K) - 1.205*\log(\varphi) \quad \text{Eq. (14)}$$

$$\text{Log (R55)} = 0.948 + 0.632*\log(K) - 1.426*\log(\varphi) \quad \text{Eq. (15)}$$

$$\text{Log (R60)} = 1.096 + 0.648*\log(K) - 1.666*\log(\varphi) \quad \text{Eq. (16)}$$

$$\text{Log (R65)} = 1.372 + 0.643*\log(K) - 1.979*\log(\varphi) \quad \text{Eq. (17)}$$

$$\text{Log (R70)} = 1.664 + 0.627*\log(K) - 2.314*\log(\varphi) \quad \text{Eq. (18)}$$

$$\text{Log (R75)} = 1.880 + 0.609*\log(K) - 2.626*\log(\varphi) \quad \text{Eq. (19)}$$

Where K is permeability (md), $\emptyset$ is porosity (%), and R is pore throat size (micron) in different percentages of non-wetting phase saturation.

In the current study, pore throat radius was calculated from capillary pressure data derived from core analysis using Washburn equation. Afterward, both the Winland (Eq. 1) and Pittman (Eq. 6 through Eq. 19) equations were utilized for calculation of pore throat radius based on core porosity and permeability data. A comparison between empirical equations and core derived R35 was reveald that the Winland equation outperforms the Pittman equation. In the light of the acceptable results of the Winland equation, pore throat radius was simulated for uncored but logged intervals. For this target, porosity was claculated from petrophysical analysis, and permeability was estimated based on neural network approach. The neural network is a dynamic and non-linear system composed of a large number of processing units (neurons) and connections between these units (Chen & Sidney, 1997). To model permeability parameters, the Feed-Forward Propagation network in Matlab software was used. Figure 4 schematically represents the network component used for this purpose, in which input data (SWE, PHIT, PHIE and SWT logs), output (permeability parameter), and 11 neurons for hidden layer were considered. In this network, hyperbolic tangent sigmoid function (TANSIG) for the transfer function of the first-to-second layer, and the linear tranfer function (Purelin) for the second-to-third layer, and the error MSE function were used. Validity of the results for performance of the neural network is approved by the plots shown in Figure 5 and Figure 6.

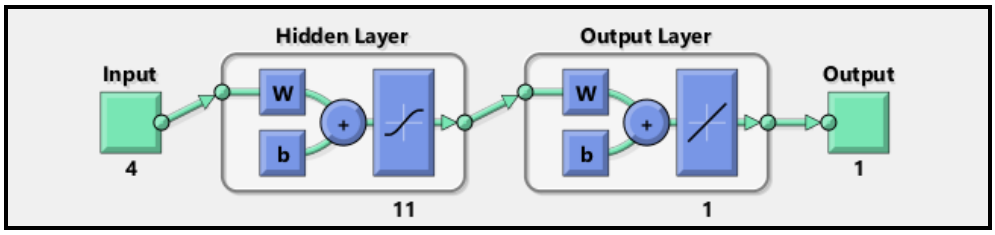

Figure 4. A schematic structure of the Feed-Forward Propagation network designed for the estimation of permeability.

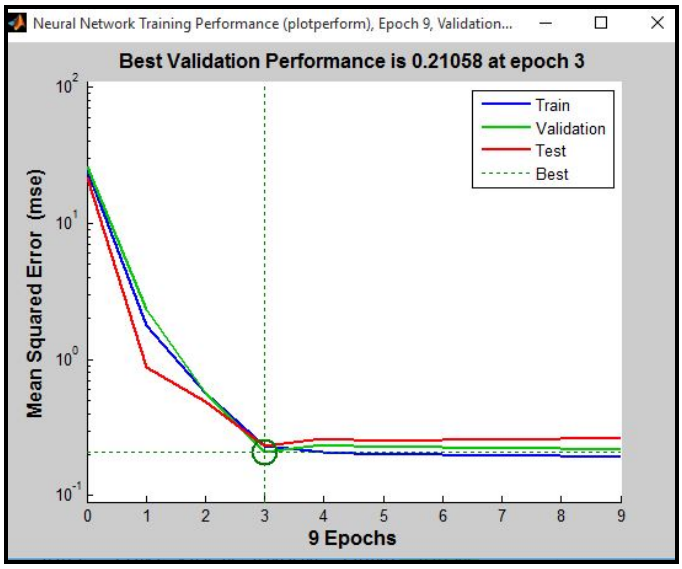

Figure 5. The mean square error in evaluation the performance of neural network for the estimation of permeability within the studied reservoir.

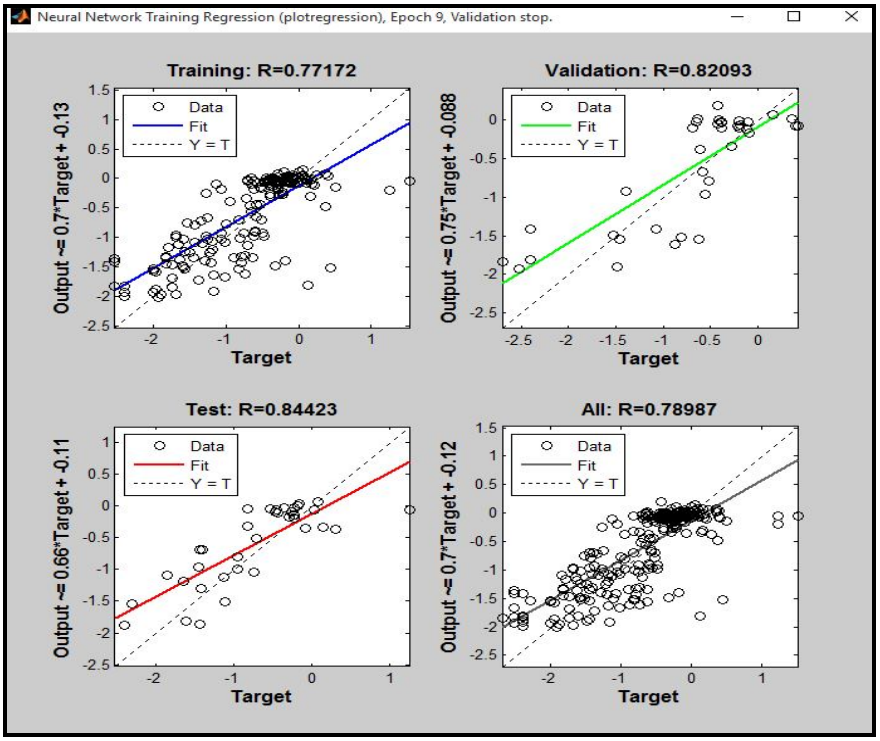

Figure 6. The good correlation between input and output data in different parts of the network for prediction of permeability within the studied reservoir.

In addition, the claculated porosity and permeability as well as generated pore throat radius as continuous logs along the studied wells are shown in Figure 7 and Figure 8. According to the Figure 7, there is a good consistency between the estimated and measured values for porosity and permeability that confirm the accuracy and reliability of the results both qualitatively (trend change) and quantitatively.

Estimation of pore throat size from seismic data

In this study, an acoustic impedance volume, obtained from 3D post-stack seismic inversion, was utilized for pore throat size estimation. Post-stack seismic inversion is an evaluation of post-stack seismic trace that tries to recreate velocity structure or acoustic impedance of the formations (Figure 9). In order to have a reliable correlation, the inversion based on linear sparse spike algorithm was taken into account.

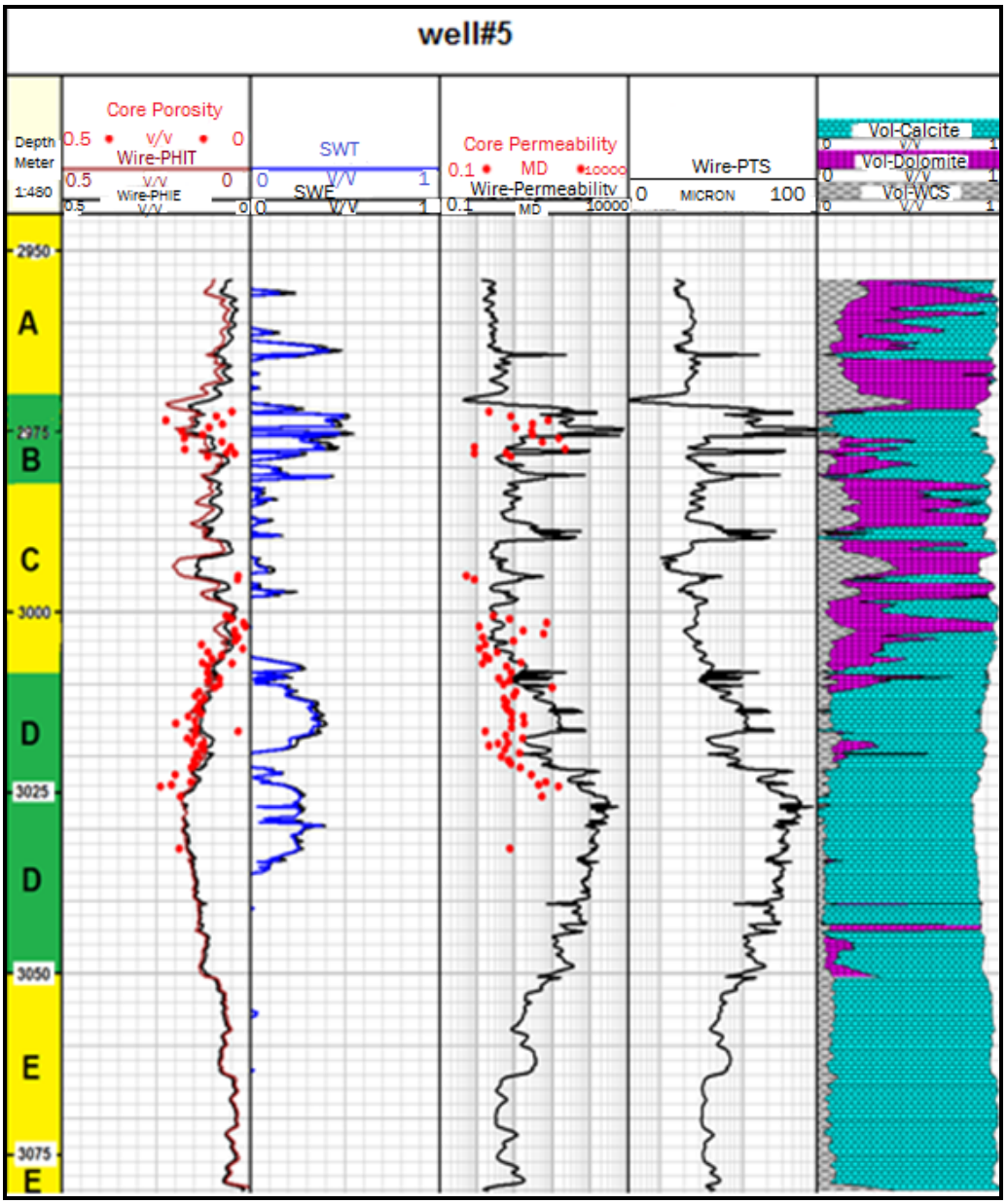

Figure 7. A comparison of core porosity (first track, red points) with effective porosity values determined by petrophysical evaluation (first track, black line) and core permeability values (the third track, red points) and the permeability determined by the artificial neural network (the third track, black line). Pore throat size (PTS) is shown in fourth track. A: Ilam zone (non-reservoir), B: Ilam_upper zone (reservoir), C: Ilam _upper-b zone (non-reservoir), D: Ilam_main zone (reservoir) and E: Ilam_poor zone (non-reservoir).

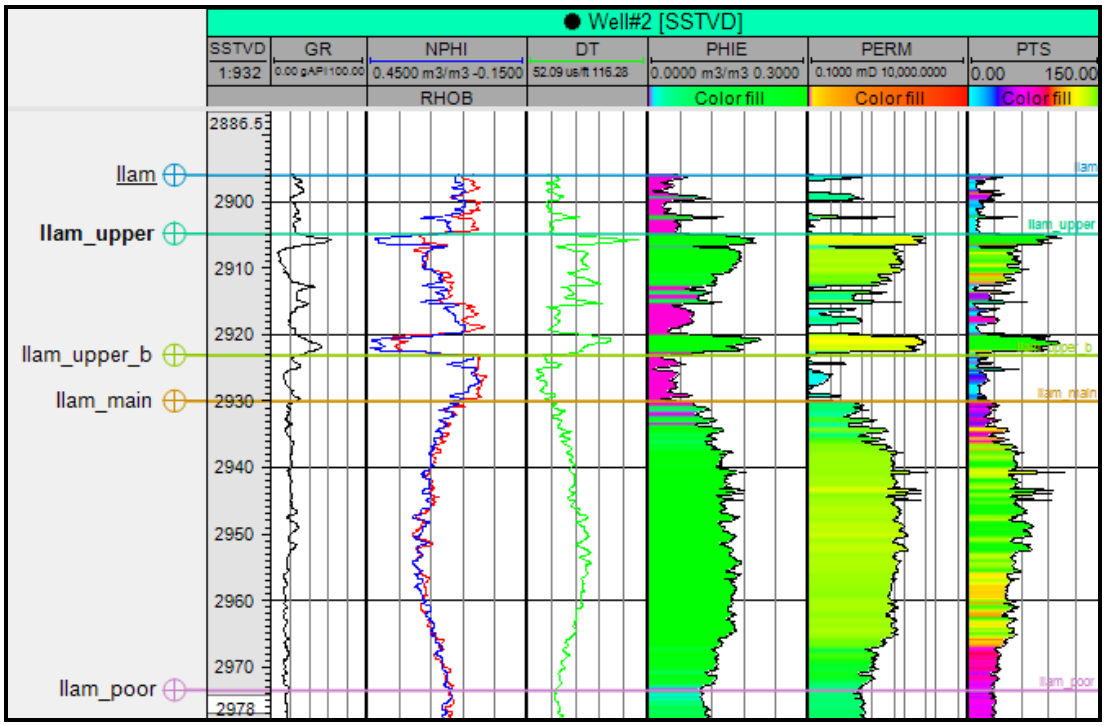

Figure 8. Correlation between the well logs and estimated porosity, permeability and generated pore throat size (PTS) within the Ilam Formation in one of the wells of the studied field.

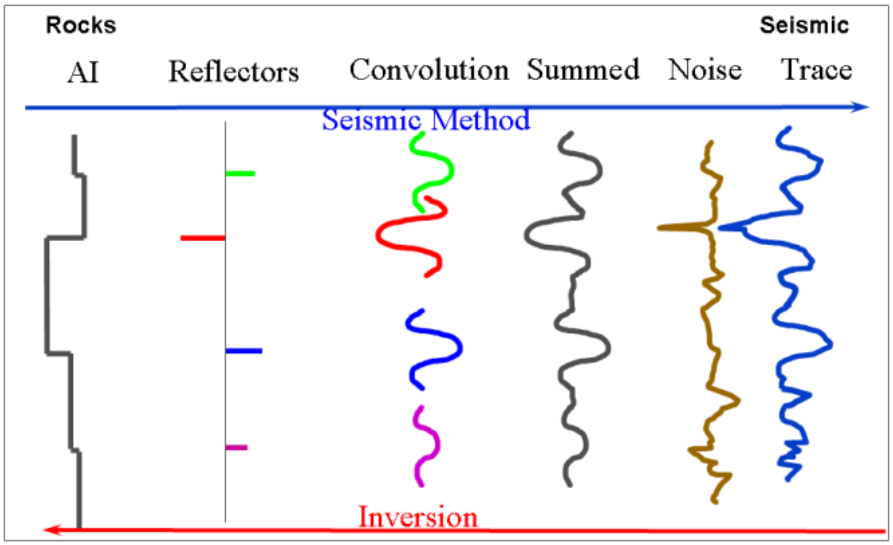

Figure 9. Mathematical representation of a geological section as a series of layers with different impedances, and the generation of a seismic record through the convolution of a source wavelet with the reflectivity series (contrasts in impedance). Inversion involves the deconvolution of the seismic traces to recover the reflectivity and then the impedance properties for the ground section (Yilmaz, 2001).

The linear sparse spike inversion is a type of model based inversion which considers the reflection ability as big spike series within the small spike context, and it seems that only the big spike are meaningful enough (Hampson *et al*., 2001).

The inversion model inputs can be divided into the following major sets:

wells coordinate information
well logs data including sonic and density logs
formation tops
seismic horizons
check shots
post stack 3D seismic data
pore throat size logs

Well to seismic tie

The recorded borehole velocity seismic data, called vertical seismic profile (VSP), were used for seismic and well transformation of well logs and seismic data in a common domain. Seismic inversion was begun with a tie of well with seismic data. As a sequence, synthetic and composite seismograms were created to measure the correlation between the well and seismic data for each individual well within a certain radius. In order to make the synthetic seismogram trace, acoustic impedance log was created by multiplication of sonic and density logs, and the reflection coefficient with convoluted seismic wavelet was calculated (Figures 10 and 11).

Seismic inversion

Seismic inversion is the name given to the process whereby geophysicists attempt to estimate the acoustic impedance (AI) of the rock layers from seismic reflection data (Russel, 1988).

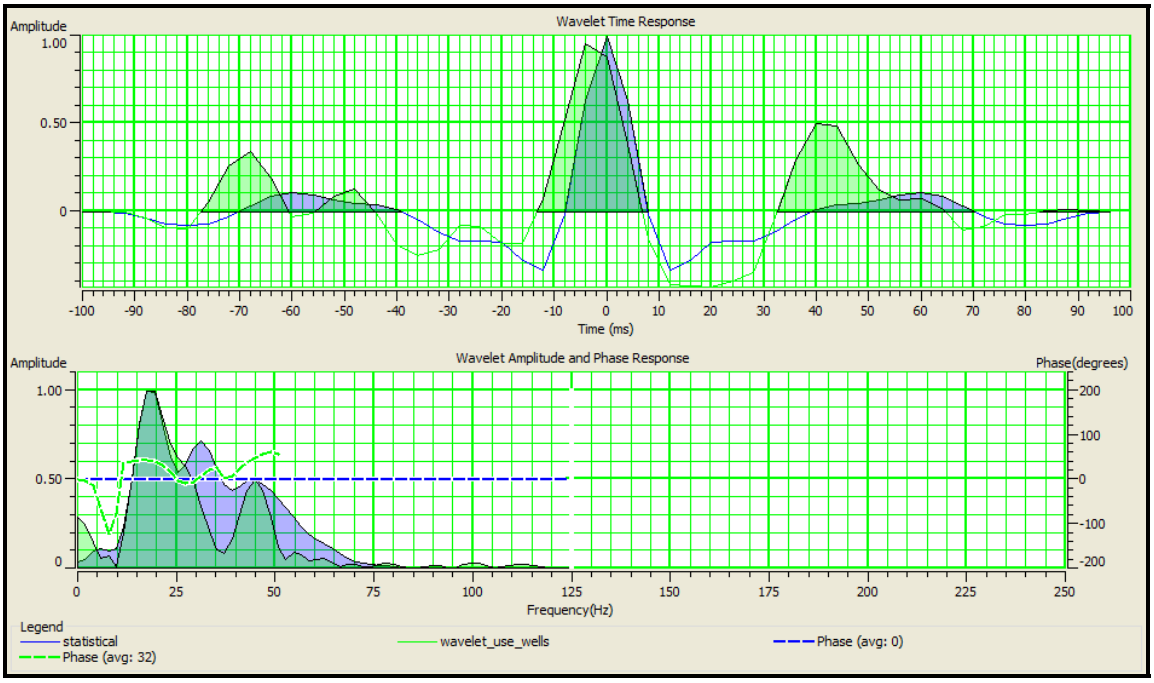

Figure 10. Amplitude phase and extracted mean wavelet used in seismic inversion.

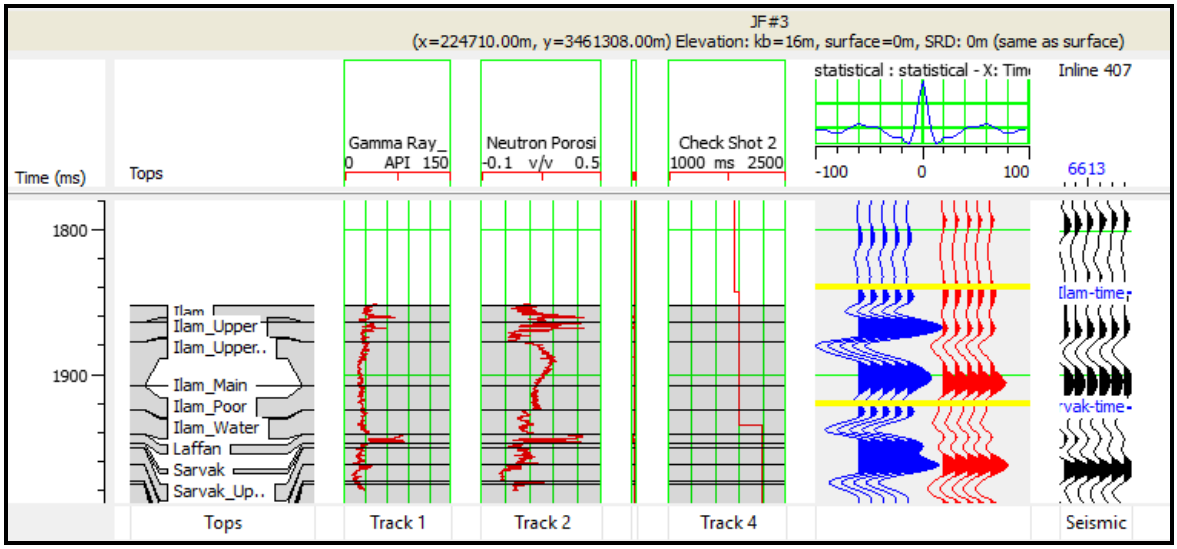

Figure 11. Well logs to seismic tie using mean seismic wavelet.

Seismic amplitude is the property of the interface between two acoustic layers. The interpretation of AI data produces more accurate and detailed structural and stratigraphic definition than seismic interpretation (HRS User's Guide, 2015). In general, this attribute has strong relationship with petrophysical properties such as lithology and porosity. Seismic inversion involves taking the observed seismic records and an estimation of the shape of the seismic pulse to obtain AI. This parameter, in contrast to the seismic data which is an indicator of the borders, investigates the whole rock layer properties (Pendrel *et al*., 2006).

The first step in seismic inversion is to generate an acoustic impedance model using well logs within the seismic horizons. After creating acoustic impedance model, different inversion algorithms (model-based, linear sparse spike, color based and etc.) are investigated. The inversion results in the studied reservoir showed that linear sparse spike algorithm outperforms other methods for acoustic impedance estimation. The inversion result based on this method has been shown in Figure 12. Also, Figure 13 illustrates a comparison between the real acoustic impedance and inversion result.

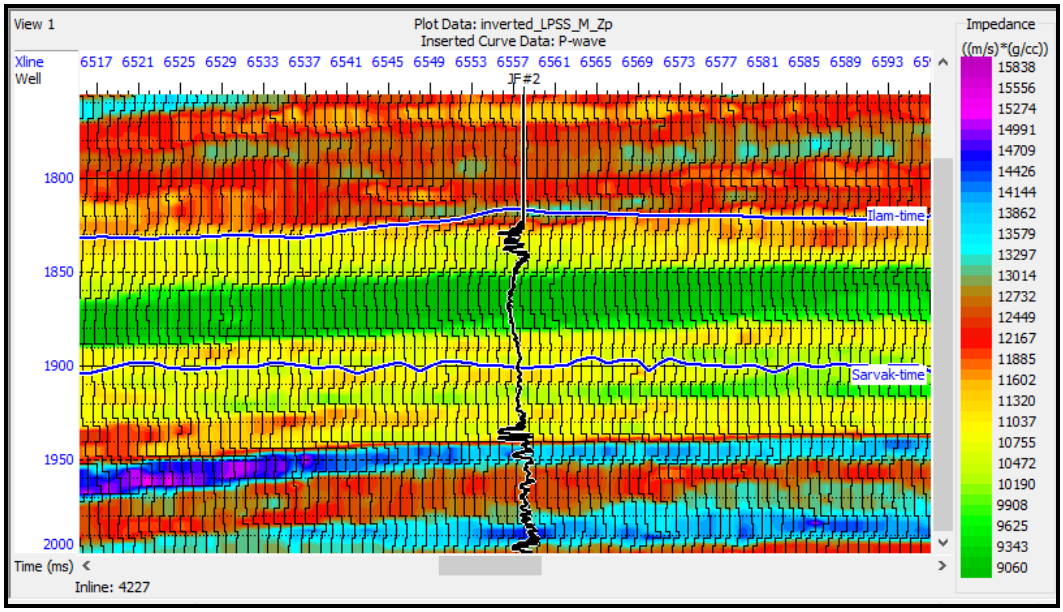

Figure 12. The resulted acoustic impedance section derived from seismic inversion based on linear spars spike algorithm around the studied wells.

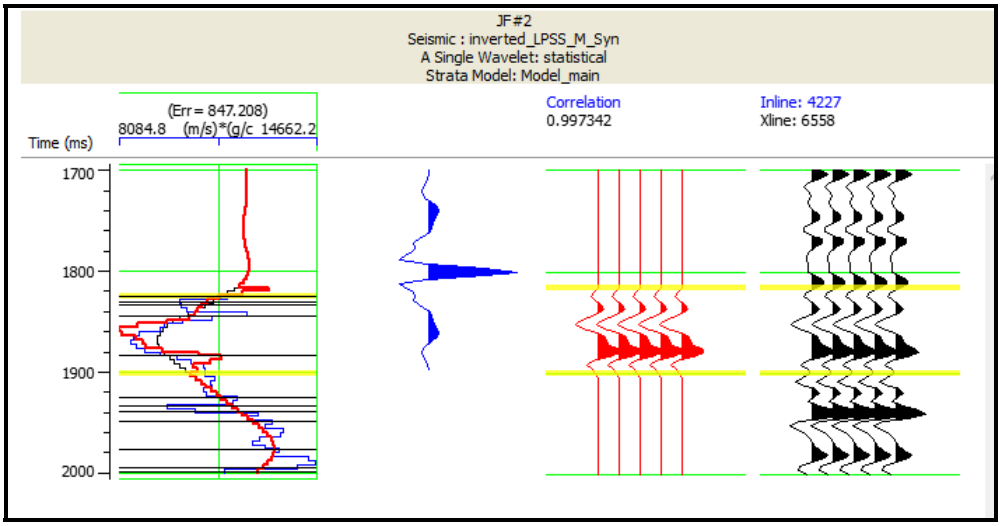

Figure 13. Correlation of real and inverted acoustic impedance based on linear sparse spike algorithm in one of the wells of the studied field.

Extraction of pore throat size cube from seismic data

The artificial neural network was used to estimate the pore throat radius by means of seismic data. In order to find the network input groups, the linear and non-linear relationships between existing input data and each output group were examined, and the groups with the best correlation with the seismic data were determined. The training and validation errors for different sets of input seismic attributes are shown in Table 1. Figure 14 demonstrates a set of input data (complex seismogram and inversion result) used for estimating R35.

There are two important issues in verification of multi-attribute analysis: first, selection of the attributes which have more relationship with the target log, and second, how to determine the optimized number of seismic attributes (Hampson *et al*., 2001).

In the most seismic inversion models, amplified operator length is used, and also the resultant frequency differences between the seismic data and well logs define the relationship between input and output data. Each sample is related to its nearest seismic sample groups, considering the high frequency of the well logs by applying the convolution operator.

In the present study, after investigating different operator length values, the best results with the lowest errors demonstrated that the most reasonable values are 5 and 6 operator lengths, respectively.

Table 1. The training and validation errors for different attributes that used for pore throat size estimation.

Target	Attributes	Training Error(micron)	Validation Error(micron)
Pore Throat Size	Acoustic Impedance	4.36	9.82
Pore Throat Size	Amplitude Envelope	5.65	10.13
Pore Throat Size	Filter 15/20-25/30	6.21	10.41
Pore Throat Size	Derivative Instantaneous Amplitude	7.01	9.39
Pore Throat Size	Integrate	8.07	10.85

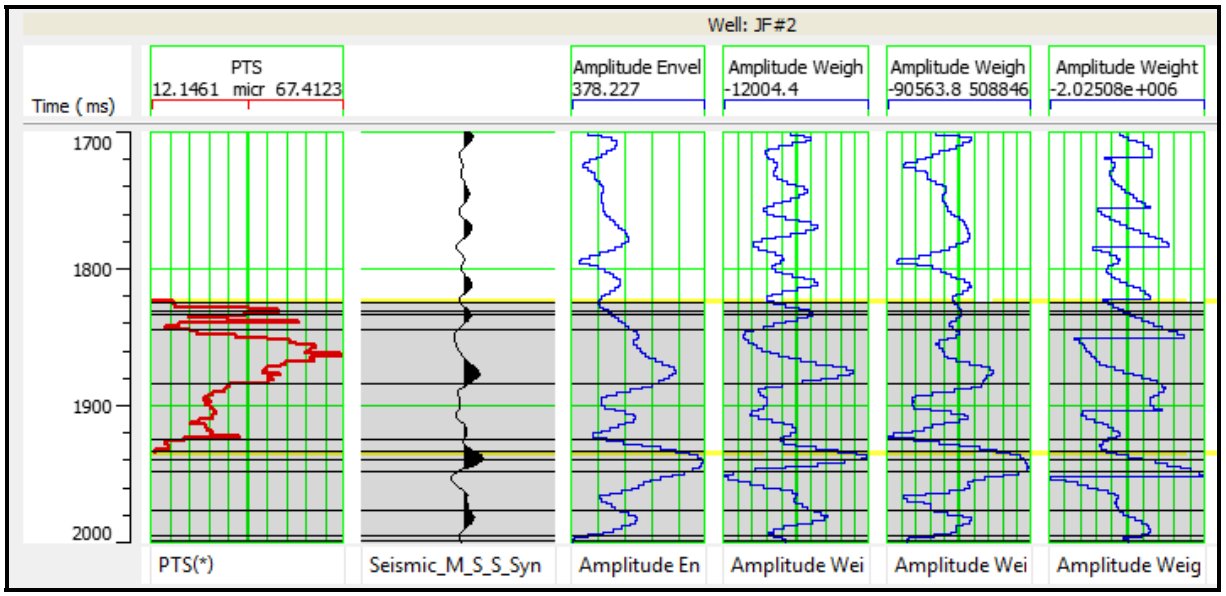

Figure 14. Graphical representation of input attributes and the target log. The target log, pore throat size, is the red line, while, complex seismogram and inversion result are shown in black and blue colors, respectively.

Then, the groups of output data achieved from regression analysis (multiple seismic attributes), were used as input of artificial neural network (ANN) model. Then, a probabilistic neural network (PNN model) was created to verify the non-linear relationship between inputs (multiple seismic attributes) and outputs (PTS: pore throat size). The correlation estimation error values were recorded for all situations. PNN was then selected as the best algorithm among other available methods according to its low estimation error and high correlation (Figure 15). As a result, by considering PNN as an optimal model, and using the optimized seismic attributes, all seismic volume was inverted to PTS. The predicted PTS from PNN model showed a similarity and reasonable correlation with actual PTS data of core samples in well locations (Figure 16 and Figure 17).

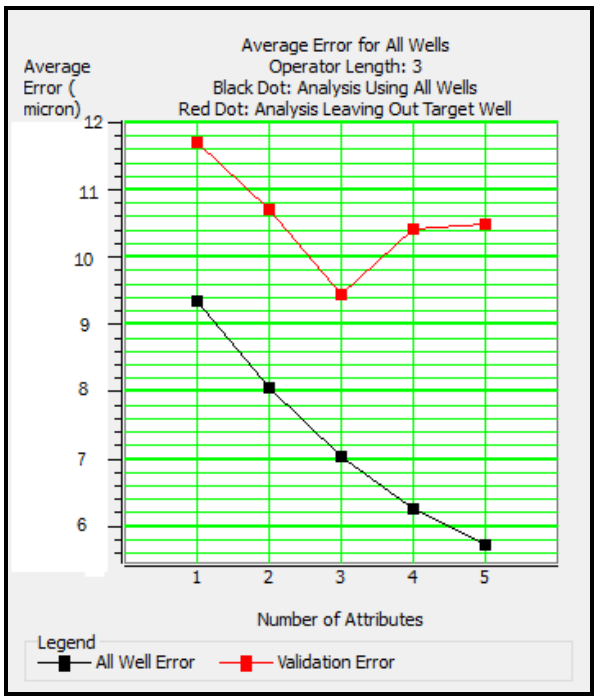

Figure 15. Validation diagram for determination of the optimal number of the attributes used in PTS prediction in the studied field.

Finally, the non-linear relationships and proved network for PTS prediction at wellbores were applied on all seismic volume.

Results and Discussion

Application a stepwise regression showed that seismic attributes including acoustic impedance, amplitude envelope, filter 15/20-25/30 and derivative instantaneous amplitude are the best predictor set for converting the 3D seismic volume into a pore size cube using a probabilistic neural network mode. Neural network algorithm improved the accuracy of the regression model for PTS estimation. The results indicated that the distribution of PTS has intimate relationship with the reservoir architecture and variations in reservoir quality within the studied interval. As variations in PTS values, is well consistent with five distinct intervals of the Ilam Formation, among which two zones (Ilam Main and Ilam Upper) have higher pore throat size and porosity than the other intervals. This corresponds with the presence of oil-bearing rocks in these zones (Figures 18 and 19). The extracted PTS maps of different zones of the Ilam Formation have been shown in Figures 20 to 22.

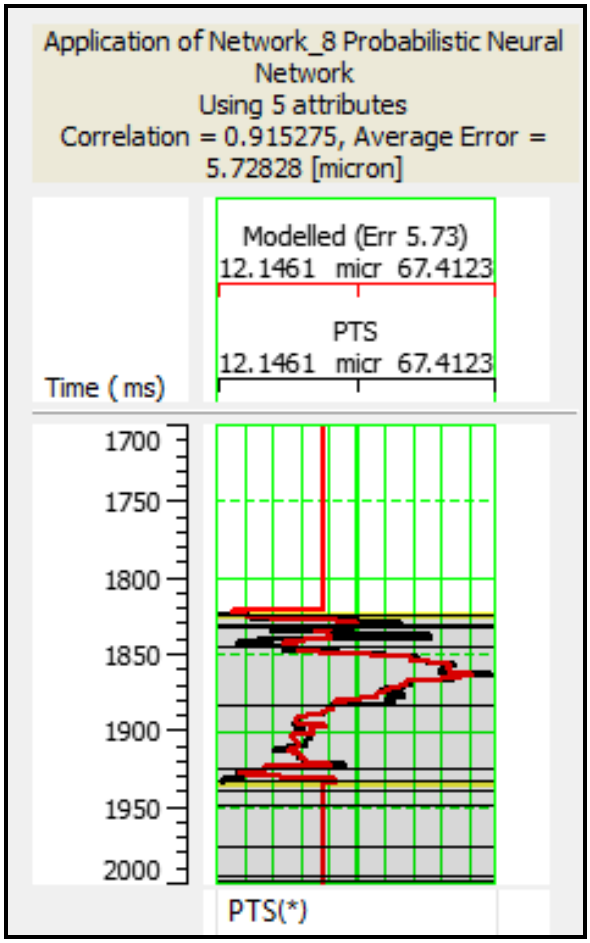

Figure 16. Plot showing the result of Artificial Neural Network algorithm for estimation of pore throat size. The red line illustrates the estimated log and the black line shows original log. According to the figure, the amount of correlation is 0.912 and the error value is less than 5.7.

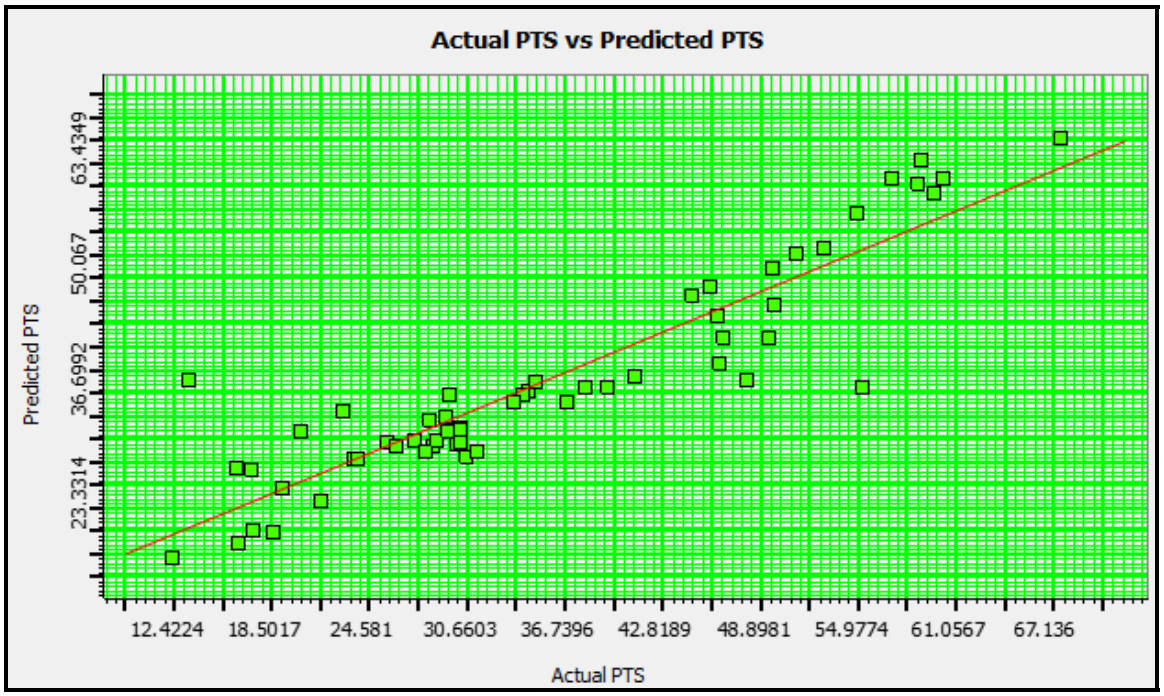

Figure 17. Cross plot showing the correlation coefficient between measured and predicted pore throat size (PTS).

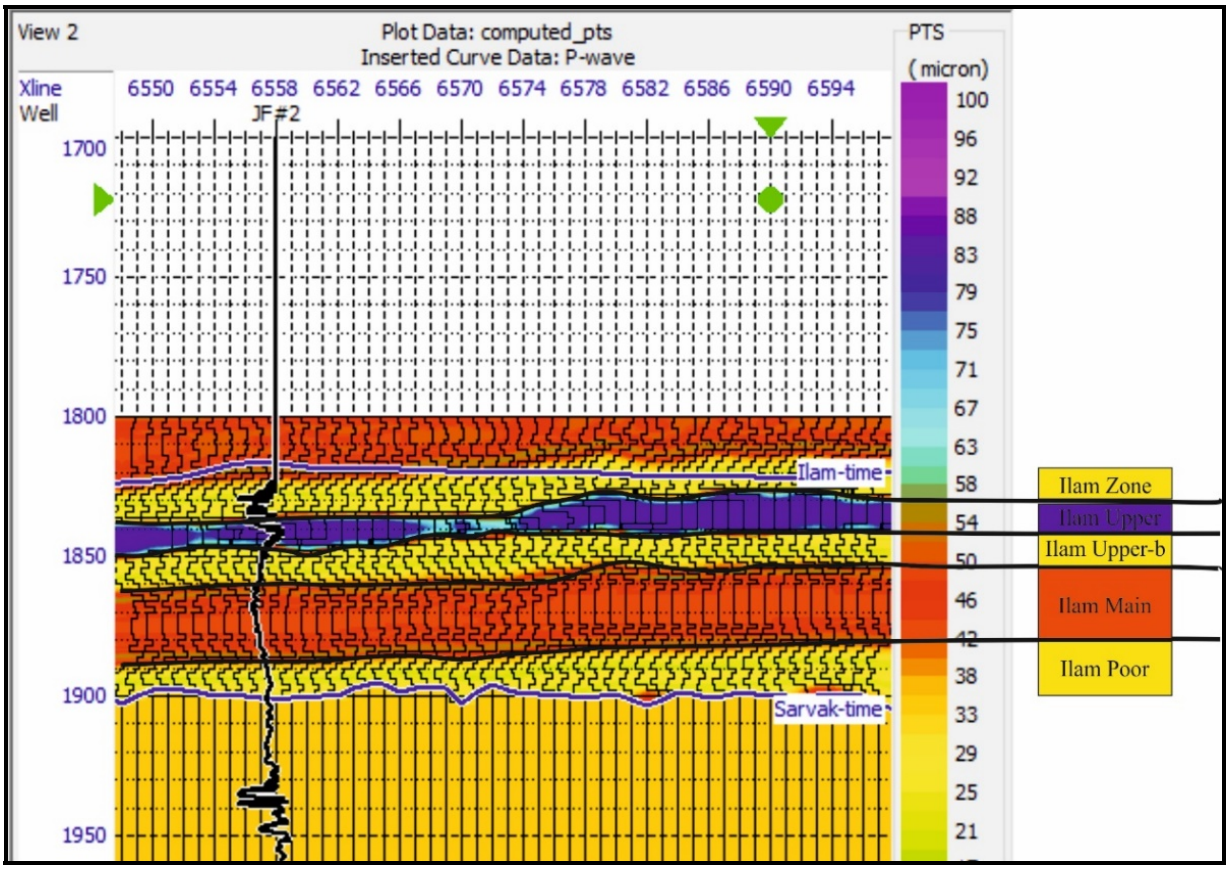

Figure 18. The extracted seismic section modeled by PNN, showing 5 distinct zones based on the distribution of pore throat size within the reservoir interval.

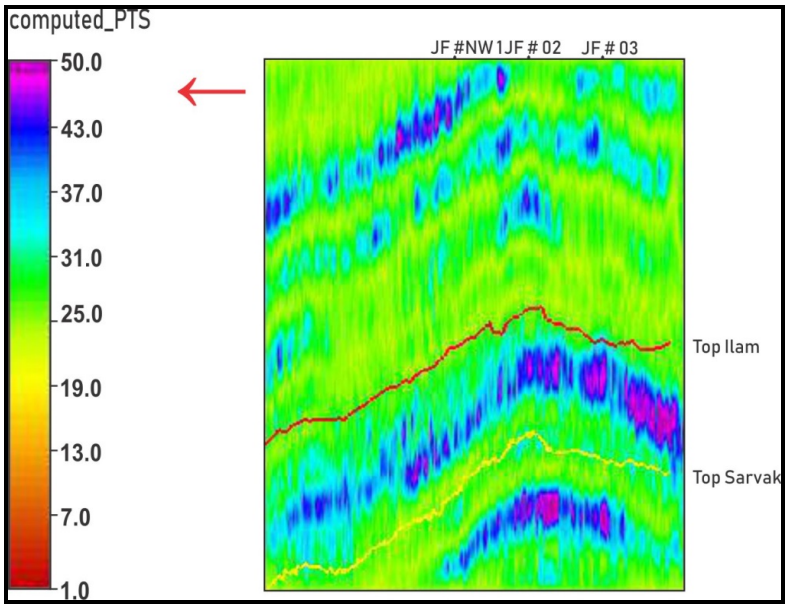

Figure 19. 3D pore throat size changes in Ilam Interval. The blue and purple parts are the main reservoir parts. The green and yellow colors show the small pore throats sizes.

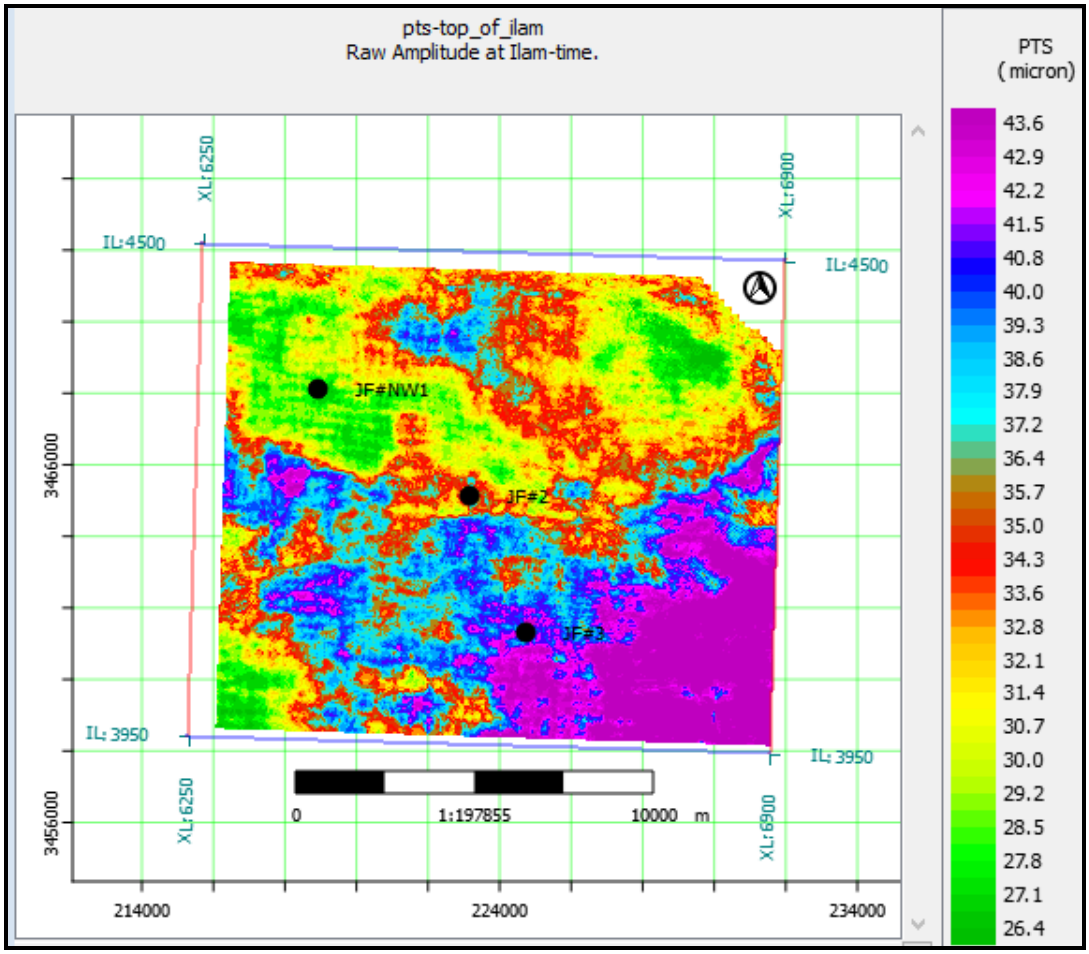

Figure 20. Pore throat size time map in top of the Ilam Formation (Ilam Zone).

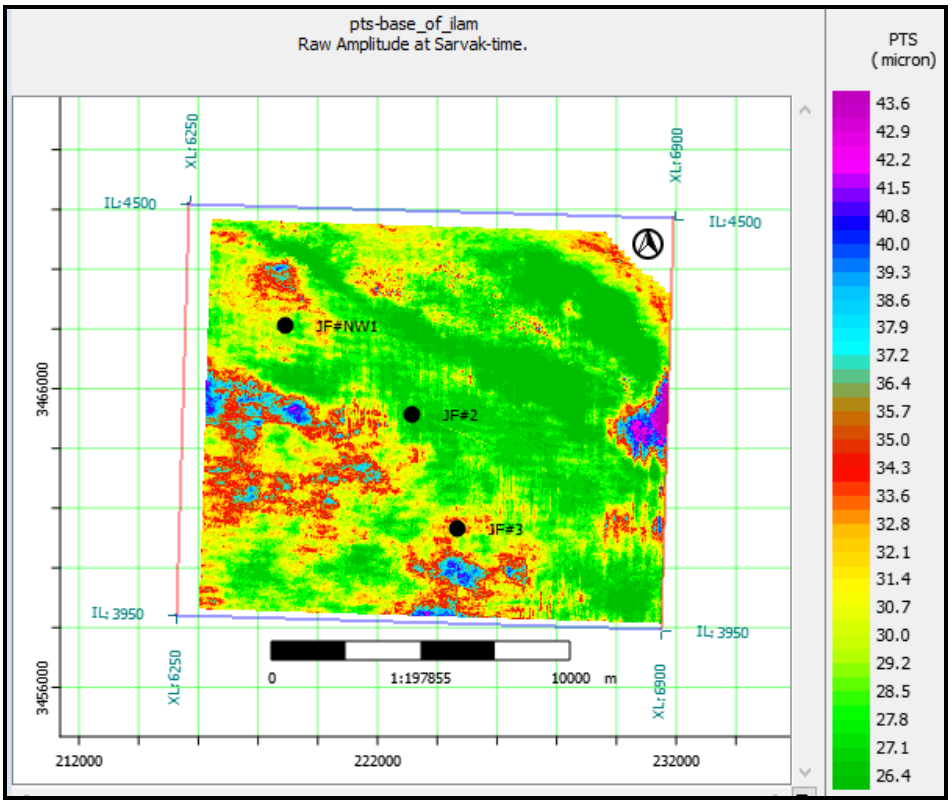

Figure 21. Pore throat size time map at the base of Ilam Formation (Ilam Poor Zone).

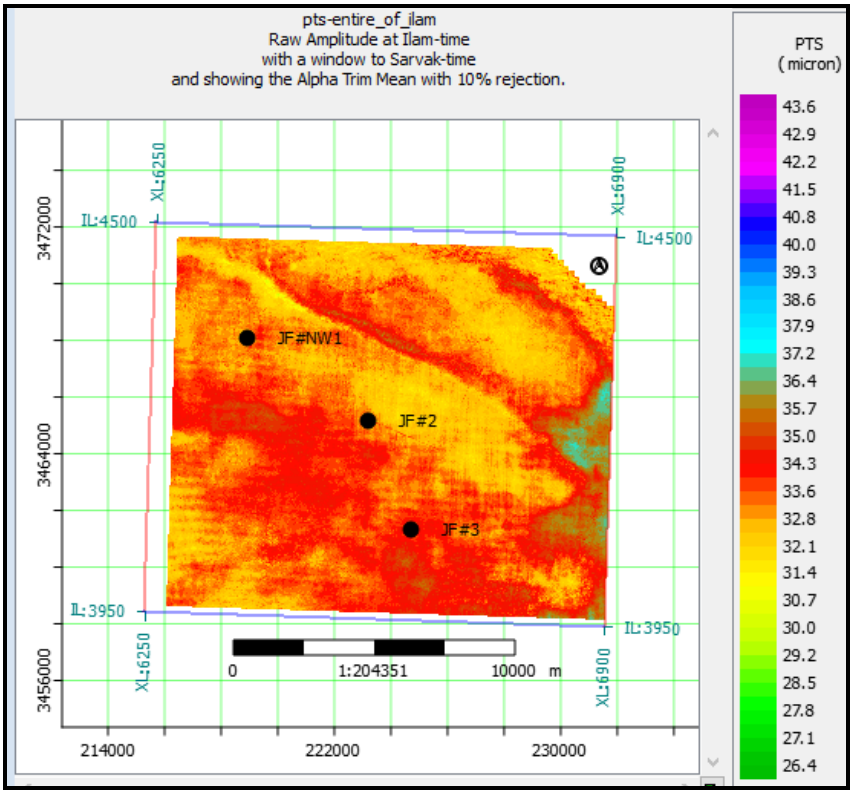

Figure 22. The average pore throat size time map in the middle of Ilam Formation (Ilam Main Zone).

Conclusion

In this study with the target of pore throat size evaluation of carbonate reservoirs, a combination of core, petrophysical logs and seismic data were used. After estimation of pore throat size using empirical equations and based on core data, the pertinent log was extracted from petrophysical well logs, and then the results were correlated with seismic data. So, the 3D volume of seismic data was inverted to acoustic impedance, by utilization a Linear Sparse Spike algorithm. Afterward, a formulation between seismic attributes and pore throat size (PTS) as target log, were established using a step-wise regression and a probabilistic neural network, which based on seismic volume was converted into pore size cube.

The results show good consistency between variations in PTS values and reservoir characteristics of reservoir zones. Among different zones of the studied formation, Ilam Main and Ilam Upper zones show higher reservoir quality in terms of their pore throat size and porosity values.

References

Asl, S.S., Aleali, M., 2016. Microfacies patterns and depositional environments of the Sarvak Formation in the Abadan Plain, Southwest of Zagros, Iran. Open Journal of Geology, 6: 201.

Bornard, R., Allo, F., Coléou, T., Freudenreich, Y., Caldwell, D. H., Hamman, J. G., 2005.Petrophysical seismic inversion to determine more accurate and precise reservoir properties (SPE94144). In67th EAGE Conference & Exhibition.

Bosch, M., Mukerji, T., Gonzalez, E. F., 2010. Seismic inversion for reservoir properties combining statistical rock physics and geostatistics: A review. Geophysics, 75: 165–176.

Buryakovsky, L., Chilingar, G. V., Rieke, H. H., Shin, S., 2012. Fundamentals of the petrophysics of oil and gas reservoirs. John Wiley & Sons.

Dai, J., Xu, H., Snyder, F., Dutta, N., 2004. Detection and estimation of gas hydrates using rock physics and seismic inversion: Examples from the northern deepwater Gulf of Mexico. The Leading Edge, 23: 60-66.

Dolberg, D. M., Helgesen, J., Hanssen, T. H., Magnus, I., Saigal, G., Pedersen, B. K., 2000. Porosity prediction from seismic inversion, Lavrans Field, Halten Terrace, Norway. The Leading Edge, 19: 392–399.

Dorrington, K. P., Link, C. A., 2004. Genetic–algorithm/neural–network approach to seismic attribute selection for well–log prediction. Geophysics, 69: 212–221.

Grana, D., Della Rossa, E., 2010. Probabilistic petrophysical–properties estimation integrating statistical rock physics with seismic inversion. Geophysics, 75: O21–O37.

Hampson, D. P., Schuelke, J. S., Quirein, J. A., 2001. Use of multiattribute transforms to predict log properties from seismic data. Geophysics, 66: 220–236.

HRS User's Guide, 2015. CGGVeritas Hampson–Russell, Calgary, Alberta, Canada.

Kolodzie, Jr, S., 1980.Analysis of pore throat size and use of the Waxman–Smits equation to determine OOIP in Spindle Field, Colorado. In SPE Annual Technical Conference and Exhibition.Society of Petroleum Engineers, 21–24.

Mehrabi, H., Rahimpour–Bonab, H., Enayati–Bidgoli, A. H., Navidtalab, A., 2014. Depositional environment and sequence stratigraphy of the Upper Cretaceous Ilam Formation in central and southern parts of the Dezful Embayment, SW Iran. Carbonates and Evaporites, 29: 263–278.

Nelson, P. H., 2009. Pore–throat sizes in sandstones, tight sandstones, and shales. AAPG Bulletin, 93: 329–340.

Pendrel, J., Mangat, C., Feroci, M., 2006.Using Bayesian inference to compute facies–fluids probabilities. In CSEG Annual Meeting, Expanded Abstracts.

Pittman, E. D., 1992. Relationship of porosity and permeability to various parameters derived from mercury injection–capillary pressure curves for sandstone. AAPG Bulletin, 76: 191–198.

Rezaee, M. R., Jafari, A., Kazemzadeh, E., 2006. Relationships between permeability, porosity and pore throat size in carbonate rocks using regression analysis and neural networks. Journal of Geophysics and Engineering, 3: 370.

Russell, B. H., 2004. The application of multivariate statistics and neural networks to the prediction of reservoir parameters using seismic attributes.

Russell, B. H., 1988. Introduction to seismic inversion methods, Society of Exploration Geophysicists.

Scott, J. B., Barker, R. D., 2003. Determining pore-throat size in Permo-Triassic sandstones from low-frequency electrical spectroscopy. Geophysical Research Letters, 30.

Sepehr, M., Cosgrove, J. W., 2004.Structural framework of the Zagros fold–thrust belt, Iran. Marine and Petroleum Geology, 21: 829–843.

Shahraeeni, M. S., Curtis, A., Chao, G., 2012. Fast probabilistic petrophysical mapping of reservoirs from 3D seismic data. Geophysics, 77: 01–019.

Tiab, D., Donaldson, E. C., 2015. Petrophysics: theory and practice of measuring reservoir rock and fluid transport properties. Gulf professional publishing.

Wardlaw, N. C., Li, Y., Forbes, D., 1987. Pore–throat size correlation from capillary pressure curves. Transport in Porous Media, 2: 597–614.
Washbourn, E. W., 1921. Note on a method of determination the distribution pore size in a porous material: Proceeding of the National Academy of Science, 7: 115–116.
Yarmohammadi, S., Kadkhodaie–Ilkhchi, A., Rahimpour–Bonab, H., Shirzadi, A., 2014. Seismic reservoir characterization of a deep water sandstone reservoir using hydraulic and electrical flow units: A case study from the Shah Deniz gas field, the South Caspian Sea. Journal of Petroleum Science and Engineering, 118: 52–60.
Yilmaz, Ö., 2001. Seismic data analysis. Society of Exploration Geophysicists, 1: 74170–2740.